

Article

# Recovery of Gold and Iron from Cyanide Tailings with a Combined Direct Reduction Roasting and Leaching Process

Pingfeng Fu <sup>1,2,\*</sup> , Zhenyu Li <sup>1</sup>, Jie Feng <sup>1</sup> and Zhenzhong Bian <sup>1</sup>

<sup>1</sup> School of Civil and Resources Engineering, University of Science and Technology Beijing, Beijing 100083, China; lizhenyu92@126.com (Z.L.); fengjie@ustb.edu.cn (J.F.); bzhenzhong@163.com (Z.B.)

<sup>2</sup> Key Laboratory of High-Efficient Mining and Safety of Metal Mines, Ministry of Education, Beijing 100083, China

\* Correspondence: pffu@ces.ustb.edu.cn; Tel.: +86-10-6233-2902

Received: 25 June 2018; Accepted: 19 July 2018; Published: 21 July 2018



**Abstract:** Cyanide tailings are the hazardous waste discharged after gold cyanidation leaching. The recovery of gold and iron from cyanide tailings was investigated with a combined direct reduction roasting and leaching process. The effects of reduction temperature, coal dosage and CaO dosage on gold enrichment into Au-Fe alloy ( $\text{Fe}_x\text{Au}_{1-x}$ ) were studied in direct reduction roasting. Gold containing iron powders, i.e., Au-Fe alloy, had the gold grade of 8.23 g/t with a recovery of 97.46%. After separating gold and iron in iron powders with sulfuric acid leaching, ferrous sulfate in the leachate was crystallized to prepare  $\text{FeSO}_4 \cdot 7\text{H}_2\text{O}$  with a yield of 222.42% to cyanide tailings. Gold enriched in acid-leaching residue with gold grade of 216.58 g/t was extracted into pregnant solution. The total gold recovery of the whole process reached as high as 94.23%. The tailings generated in the magnetic separation of roasted products, with a yield of 51.33% to cyanide tailings, had no toxic cyanide any more. The gold enrichment behaviors indicated that higher reduction temperature and larger dosage of coal and CaO could promote the allocation of more gold in iron phase rather than in slag phase. The mechanism for enriching gold from cyanide tailings into iron phase was proposed. This work provided a novel route to simultaneously recover gold and iron from cyanide tailings.

**Keywords:** cyanide tailings; hazardous waste; direct reduction roasting; Au-Fe alloy; acid leaching; gold recovery

## 1. Introduction

Cyanidation leaching, which discharges a great amount of cyanide tailings, is the predominant process to produce gold around the world [1,2]. As toxic cyanides and heavy metals such as mercury and arsenic remain in cyanide tailings, they are extremely harmful to human beings and animals, and are classified as hazardous wastes in China [3–7]. Nevertheless, the content of valuable metals such as gold and iron may be high in cyanide tailings. The gold grade and total iron (TFe) content of some tailings can reach 3–9 g/t and above 30%, respectively [8–10]. Therefore, attention should be paid to recovering valuable metals from cyanide tailings [11–15].

Since sulfide minerals are still present in cyanide residues discharged after direct cyanidation leaching, flotation is an efficient method to recover noble metals and non-ferrous metals such as Cu, Zn and Pb [16–18]. However, noble metals in cyanide tailings discharged after the roasting-cyanidation leaching are enclosed in iron oxide minerals (e.g., hematite). To recover iron in the tailings, the magnetization roasting-magnetic separation is investigated to produce iron concentrates by reducing

hematite to magnetite. However, some reports showed that the TFe content of iron concentrates was below 60% due to high content of impurities such as  $\text{SiO}_2$  and  $\text{Al}_2\text{O}_3$  [8]. The acid-leaching ammonia process was also tested to dissolve iron oxides in cyanide tailings with nitric or sulfuric acid and to prepare iron oxide pigments [19].

To recover noble metals in cyanide tailings, magnetization roasting is applied to promote gold extraction, and the gold leaching rate of 46.14% was reported [9]. However, magnetite in roasted products is found to have a negative effect on gold leaching, which leads to low Au leaching rate [20]. Since the gold can react with  $\text{Cl}_2$  or  $\text{HCl}$  to generate volatile gold chlorides at high temperature, the chlorination roasting has been studied to recover gold from cyanide tailings with the gold recovery of above 90% [21,22]. However, this process has deficiencies involving  $\text{Cl}_2$  and  $\text{HCl}$  gases which can corrode the equipment and is extremely harmful to human health.

Up to now, the simultaneous recovery of gold and iron from cyanide tailings has rarely been investigated. Although acid leaching can achieve high gold recovery and produce  $\text{FeSO}_4$  or iron oxide pigments [19], this process is complex and costly due to large acid consumption and severe leaching conditions. Magnetization roasting can promote the recovery of iron and gold from cyanide tailings, but the gold recovery is quite low [9,20]. Therefore, it is necessary to develop an efficient and feasible process to recover gold and iron from cyanide tailings after the roasting-cyanidation leaching.

Atomic Au and Fe can form Au-Fe alloys at high temperature [23]. The unique electrical [24], magnetic [25], thermodynamic [26] and catalytic [27] properties of Au-Fe alloys have attracted great interest. It suggests that gold remains in cyanide tailings can be captured and enriched in metallic iron if a high-temperature reduction process is conducted. The direct reduction-magnetic separation can effectively recover iron from converter slag [28], vanadium tailings [29], copper slag [30,31], and lead smelting slag [32] to produce iron powders. In this work, direct reduction roasting is applied to produce gold containing iron powders, namely Fe-rich Au-Fe alloy ( $\text{Fe}_x\text{Au}_{1-x}$ ), from cyanide tailings. The gold and iron in iron powders are separated by sulfuric acid leaching. Then the leachate is used to produce  $\text{FeSO}_4 \cdot 7\text{H}_2\text{O}$  crystals with a low temperature crystallization method. Although the extraction of gold with alternative lixiviants (e.g., thiosulfate and bromide) do not produce cyanide residue [33,34], the cyanidation extraction is conducted to recover gold from acid-leaching residue because generated cyanide residue can be recycled as raw materials into direct reduction roasting, thus no secondary cyanide residue is produced in this process.

The objectives of this study are: (1) to evaluate the technical feasibility of simultaneous recovery of gold and iron from cyanide tailings via the combined direct reduction roasting and leaching process; (2) to investigate the effects of reduction temperature, coal dosage and  $\text{CaO}$  dosage on the enrichment of gold into Au-Fe alloy in direct reduction roasting; and (3) to propose the mechanism for gold enrichment from cyanide tailings into iron phase. The results in this work can provide a novel route to effectively recover gold and iron from cyanide tailings, pyrite cinders and gold containing iron ores.

## 2. Materials and Methods

### 2.1. Materials and Reagents

The cyanide tailings discharged after the roasting-cyanidation leaching were received from a gold smelting plant in Henan Province, China. The main chemical composition was given in Table 1. The TFe content and gold grade reached 44.96% and 3.83 g/t, respectively, indicating high content of valuable metals. The mineral composition revealed by X-ray powder diffraction (XRD) (Figure 1) indicated that dominant minerals were hematite and quartz. The coal with a size of less than 0.5 mm, used as the reducing agent, had 9.81% of ash, 26.34% of volatiles, 0.73% of moisture and 63.12% of fixed carbon based on its industrial analysis. The  $\text{CaO}$  in analytical grade was purchased from Sinopharm Chemical Reagent Co., Ltd. The  $\text{CaO}$  content was higher than 98.0% as given by the supplier.

**Table 1.** Main chemical composition of received cyanide tailings.

Components	TFe	Au *	SiO <sub>2</sub>	Al <sub>2</sub> O <sub>3</sub>	CaO	MgO	Na <sub>2</sub> O	K <sub>2</sub> O
Content (%)	44.96	3.83	24.35	2.47	0.58	0.67	1.26	1.15

\* The unit of Au was g/t.

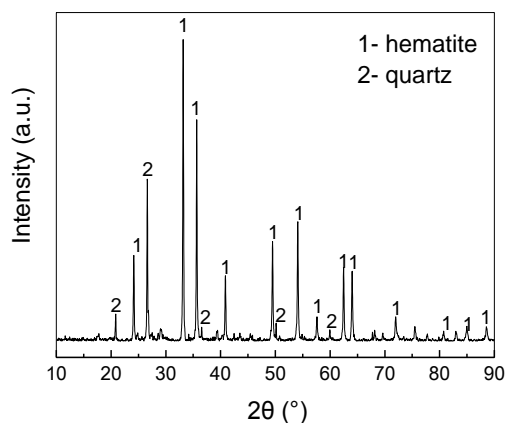


**Figure 1.** XRD pattern of received cyanide tailings.

### 2.2. Direct Reduction Roasting of Cyanide Tailings

The recovery process was shown in Figure 2. Cyanide tailings were dried at 105 °C overnight. 30 g tailings were thoroughly mixed with coal and CaO with a designated dosage. Herein, the dosage of coal or CaO was expressed by a percentage that referred to its mass ratio to cyanide tailings. The dosages of coal and CaO were chosen in the range from 8.0 wt.% to 20 wt.% and from 5 wt.% to 20 wt.%, respectively. The mixture was added to a graphite crucible with a lip. The direct reduction roasting was conducted in a muffle furnace (CD-1400X, Zhengzhou Chida Tungsten & Molybdenum Products Co. Ltd., Zhengzhou, China). When the reduction temperature reached its designated value of 1050–1250 °C, the crucible was transferred into the furnace and maintained for 90 min at a reduction atmosphere. After that, the crucible was taken out of the furnace and cooled down to room temperature in air.

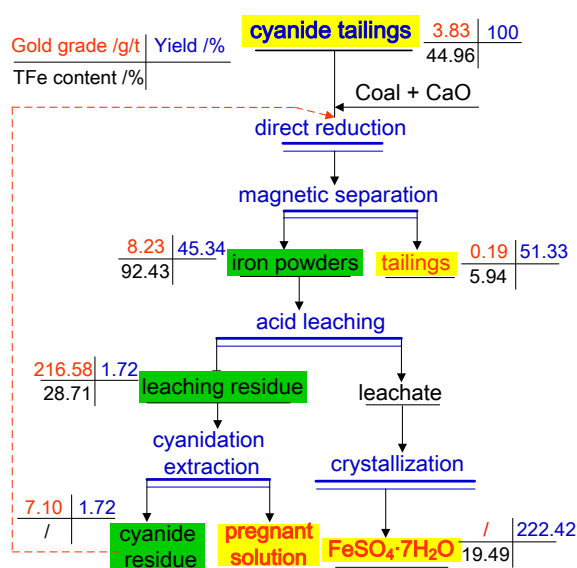


**Figure 2.** Flowsheet for the recovery of gold and iron from cyanide tailings at the reduction temperature of 1200 °C. (The Yield is defined as the weight percentage of solid products to received cyanide tailings as shown in Equation (5)).

The roasted product was firstly ground to lower than 0.074 mm fraction of 70.2% in a rod mill (RK/BM, Wuhan Rock Crush & Grand Equipment Manufacture Co., Ltd., Wuhan, China), then separated by a magnetic tube separator (XCGS-73, Xinsheng Mining Equipment Co., Ltd., Jiangxi, China) at a field intensity of 167.06 kA/m. The concentrate was further ground to lower than 0.045 mm fraction of 80.5% and separated at 107.41 kA/m to obtain final iron concentrate, i.e., reduced iron powders containing gold. The tailings generated in two stage magnetic separation as shown in Figure 2 were collected as magnetic separation tailings. The TFe or gold recovery of reduced iron powders was calculated as follows:

$$\varepsilon = \frac{W_1 \times \beta_1}{W_0 \times \beta_0} \times 100\% \quad (1)$$

where,  $\varepsilon$  was the TFe or gold recovery (%),  $W_1$  was the weight of reduced iron powders (g),  $\beta_1$  was the TFe content (%) or gold grade (g/t) of iron powders,  $W_0$  was the weight of cyanide tailings (g), and  $\beta_0$  was the TFe content (%) or gold grade (g/t) of cyanide tailings.

### 2.3. Sulfuric Acid Leaching and Preparation of Ferrous Sulfate Crystals

10 g reduced iron powders were mixed with 140 mL of 2.35 mol/L  $\text{H}_2\text{SO}_4$  solution in a conical flask. The acid leaching was performed at different temperatures for 1 h in a thermostatic bath. After the leaching, the pulp was filtered to obtain leaching residue with enriched gold. The hot leachate was firstly condensed by heating at 100 °C. After cooling down to room temperature, the condensed leachate was kept in a refrigerator at 0 °C for 12 h to crystallize  $\text{FeSO}_4 \cdot 7\text{H}_2\text{O}$ . Herein, the weight loss ratio ( $\eta$ ) and iron leaching rate ( $\gamma$ ), calculated as Equations (2) and (3), were used to evaluate acid-leaching process, respectively.

$$\eta = \frac{W_1 - W_3}{W_1} \times 100\% \quad (2)$$

$$\gamma = \frac{W_1 \times \beta_1 - W_3 \times \beta_3}{W_1 \times \beta_1} \times 100\% \quad (3)$$

where,  $\eta$  and  $\gamma$  were the weight loss ratio (%) and iron leaching rate (%), respectively,  $W_3$  was the weight of acid-leaching residue (g),  $\beta_3$  was the TFe content (%) of acid-leaching residue.

### 2.4. Cyanidation Extraction of Gold from Acid-Leaching Residue

The gold enriched in acid-leaching residue was finally recovered by cyanidation extraction. The extraction was conducted in a conical flask without air bubbling and stirred with a magnetic stirrer at 300 rpm for 36 h. The liquid to solid mass ratio was set to 10:1, and pulp pH was 11.0. The cyanide dosage was in a range of 5–80 kg/t. After the leaching, the pulp was filtered to obtain pregnant solution. The cyanide residue was dried to assay gold grade. The Au extraction rate ( $\phi$ ) was calculated as follows:

$$\phi = \frac{W_3 \times \beta_3 - W_5 \times \beta_5}{W_3 \times \beta_3} \times 100\% \quad (4)$$

where,  $\phi$  was the gold extraction rate (%),  $\beta_3$  and  $\beta_5$  was the gold grade (g/t) of acid-leaching residue and cyanide residue, respectively,  $W_5$  was the weight (g) of cyanide residue.

In this process, the yield ( $\delta_i$ ) of solid products to cyanide tailings in Figure 1 was defined as Equation (5):

$$\delta_i = \frac{W_i}{W_0} \times 100\% \quad (5)$$

where,  $W_i$  (i.e.,  $W_0$ ,  $W_1$ ,  $W_2$ ,  $W_3$ ,  $W_4$  and  $W_5$ ) was the weight (g) of cyanide tailings, iron powders, magnetic separation tailings, acid-leaching residue,  $\text{FeSO}_4 \cdot 7\text{H}_2\text{O}$  crystals and cyanide residue, respectively.

## 2.5. Analysis and Characterization

The Au grade of solid products was determined by inductively coupled plasma-optical emission spectrometry (ICP-OES, iCAP 7000, Thermo Fisher Scientific Inc., Waltham, MA, USA) at radio frequency (RF) power of 1.35 kW, air flow rate of 14 mL/min, and argon auxiliary flow rate of 0.3 mL/min. 0.3 g samples were digested with 3 mL ionized water, 9 mL HCl and 3 mL HNO<sub>3</sub> at 130 °C for 15 min in a closed microwave acid digester (DS-360x, Grand Analytical Instrument Co. Ltd., Guangzhou, China). The TFe content of solid products was analyzed by a titanium (III) chloride reduction and potassium dichromate titration method (Chinese standard, GB/T 6730.65-2009). The contents of SiO<sub>2</sub>, Al<sub>2</sub>O<sub>3</sub>, CaO, MgO, Na<sub>2</sub>O and K<sub>2</sub>O in cyanide tailings, and of Mn, Pb, As, Si, Al, and Cu in FeSO<sub>4</sub>·7H<sub>2</sub>O crystals were also obtained by ICP-OES. The mineral compositions of cyanide tailings, roasted products and acid-leaching residue were investigated by XRD (DMax-RB, Rigaku Corporation, Tokyo, Japan) under the conditions of 40 kV, 100 mA and Cu K $\alpha$  radiation. The morphology of roasted products was performed with scanning electron microscopy (SEM, EVO18, Carl Zeiss Group Corporation, Oberkochen, Germany). Roasted products were mounted on epoxy resin and further polished before the SEM observation.

## 3. Results and Discussion

### 3.1. Recovery of Gold and Iron with Direct Reduction Roasting

#### 3.1.1. Effect of Reduction Temperature

As shown in Figure 3, the TFe content and recovery of reduced iron powders were increased from 68.84% to 92.43% and from 78.98% to 93.19%, respectively, as the temperature was raised from 1050 to 1200 °C. It suggests that high temperature can promote the reduction of iron oxides to metallic iron. Meanwhile, the gold recovery was increased from 74.33% to 95.03%, indicating the enrichment of remained gold in the tailings into iron powders. As the temperature was raised up to 1250 °C, the gold recovery was further increased to 95.70%. It clearly indicated that higher temperature could promote the capture of more gold by in situ generated metallic iron.

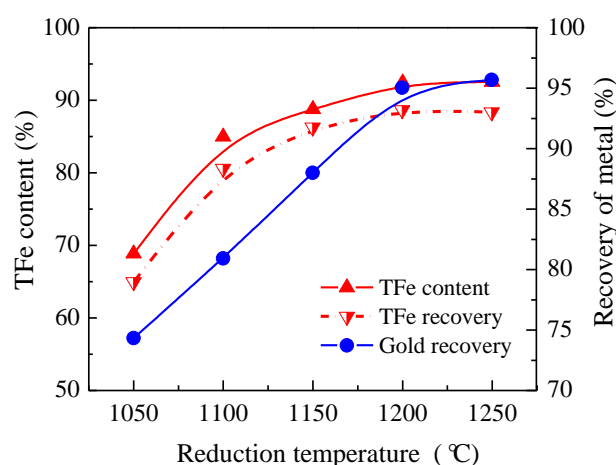


**Figure 3.** Effect of reduction temperature on the recovery of iron and gold from cyanide tailings. (Reduction conditions: reduction time of 90 min, coal dosage of 20 wt.% and CaO dosage of 15 wt.%).

The direct reduction of hematite to metallic iron generally follows the pathway of Fe<sub>2</sub>O<sub>3</sub> → Fe<sub>3</sub>O<sub>4</sub> → FeO → Fe [35]. At above 900 °C, Fe<sub>3</sub>O<sub>4</sub> can be further reduced to FeO. As the reduction of FeO to metallic iron is a strong endothermic reaction, high temperature is necessary to generate metallic iron. Due to the existence of SiO<sub>2</sub> in cyanide tailings, FeO can react with SiO<sub>2</sub> to form fayalite, a low melting point material promoting to form molten slag [36]. The amount of molten slag increase sharply at

above 1140 °C, which can facilitate the growth of iron grains and enhance the separation of iron grains from slag [37,38]. Therefore, as shown in Figure 3, the elevated temperature could increase the TFe content and recovery of iron powders.

### 3.1.2. Effect of Coal Dosage

As shown in Figure 4, when the coal dosage was increased from 8 wt.% to 20 wt.%, the TFe and gold recovery was rapidly increased from 56.36% to 93.03% and from 42.53% to 93.19%, respectively. However, the TFe content of iron powders was just increased from 89.92% to 92.43%. When the dosage was further raised up to 25 wt.%, the TFe content slightly decreased, but almost no change of the TFe and gold recovery was observed. Thus, the optimum coal dosage was 20 wt.%. The result revealed that higher coal dosage could promote to recover gold and iron from cyanide tailings.

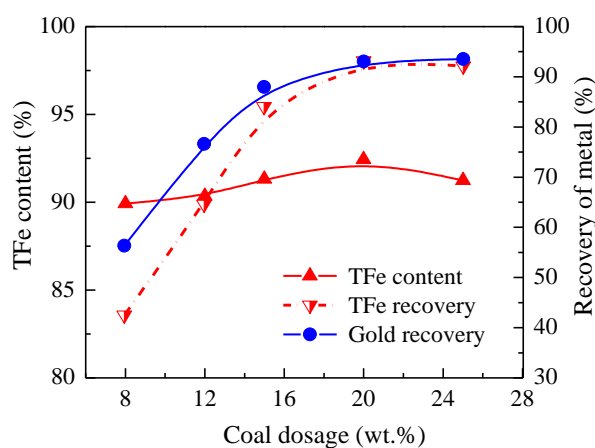


**Figure 4.** Effect of coal dosage on the recovery of iron and gold from cyanide tailings. (Reduction conditions: reduction temperature of 1200 °C, reduction time of 90 min, CaO dosage of 15 wt.%).

The high coal dosage can increase the C/O (fixed carbon/oxygen) ratio in the reduction system, which enhances the reduction atmosphere and promotes the reduction of more FeO to metallic iron [39]. Thus, the higher amount of metallic iron can surely capture more gold. The FeO in reduction system is a substance decreasing the liquidus temperature by forming a fayalite-type slag [38,40]. When more FeO was reduced to Fe at higher C/O ratio, the molten slag became less, which might reduce the mechanical mixing of gold and slag in slag phase. Therefore, the allocation of gold in metallic iron phase should be enhanced.

### 3.1.3. Effect of CaO Dosage

As shown in Figure 5, when the CaO dosage was increased from 5 wt.% to 20 wt.%, the TFe recovery was raised slightly, but the Au recovery significantly was raised from 77.65% to 97.46%. The TFe content showed a weak relationship with CaO dosage. Thus, the optimum CaO dosage was 20 wt.%. The result revealed that the CaO dosage had a remarkable effect on the gold recovery.

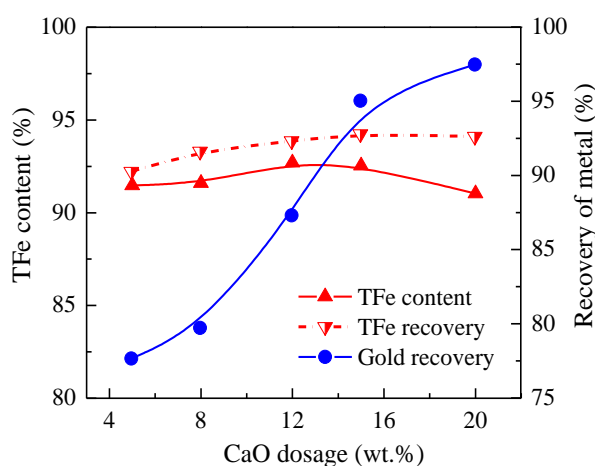
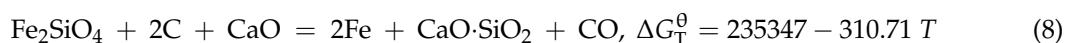
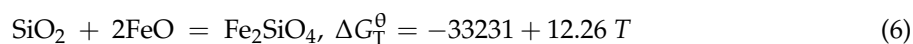


**Figure 5.** Effect of CaO dosage on the recovery of iron and gold from cyanide tailings. (Reduction conditions: reduction temperature of 1200 °C, reduction time of 90 min, coal dosage of 20 wt.%).

The SiO<sub>2</sub> content in cyanide tailings reached 24.35% as shown in Table 1. Reactive FeO can react with SiO<sub>2</sub> to form fayalite at high temperature (Equation (6)), which hinders the reduction of FeO to metallic Fe. While the CaO is added, the fayalite may readily react with fixed carbon and/or CaO to form Fe and wollastonite (Equations (7) and (8)) [41,42], which generates more metallic iron. The results revealed that higher alkalinity ( $w(\text{CaO})/w(\text{SiO}_2)$ ) of slag phase could promote more gold allocated in iron phase rather than in slag phase.



Under the optimum reduction roasting conditions: roasting temperature of 1200 °C, roasting time of 90 min, coal dosage of 20 wt.% and CaO dosage of 20 wt.%, iron powders with TFe content of 92.43% and gold grade of 8.23 g/t were achieved. The TFe and gold recovery in the direct reduction roasting reached 93.21% and 97.46%, respectively. As toxic cyanides were decomposed at 1200 °C, the magnetic separation tailings would not contain cyanides. Thus, magnetic separation tailings had lower toxicity and weight (a yield of 51.33% to cyanide tailings) compared to cyanide tailings.

### 3.2. Proposed Mechanism for Enrichment of Gold from Cyanide Tailings

Figure 6 showed the phase diagram of Au-Fe binary system [23]. Pure Au and  $\gamma$ -Fe crystals have same space groups (Fm3m) and close lattice parameters (0.40784 nm for Au and 0.36468 nm for  $\gamma$ -Fe). As shown in Figure 6, Au and  $\gamma$ -Fe atoms can form Au-rich fcc terminal solid solution (Au) and Fe-rich  $\gamma$  terminal solid solution based on fcc phase of Fe ( $\gamma$ -Fe) at high temperature [23,43]. The solubility limit of Au in the ( $\gamma$ -Fe) phase was reported to be 4.1–8.1 at.% [23]. The liquidus (L) of Au-Fe system has a minimum of 1036 °C and 18.5 at.% of Fe. In this work, when roasted in 1050 °C, remained gold in cyanide tailings may react with in situ generated  $\gamma$ -Fe to form Au-rich (Au) phase or liquidus (L) even the reduction temperature was below the melting point of pure gold (1064.43 °C). As the roasting time was extended, more  $\gamma$ -Fe was generated by the reduction of FeO, promoting the formation of ( $\gamma$ -Fe) phase with low composition of Au. When the roasting temperature was increased over the gold melting point, solid gold particles in the reduction system became molten, increasing the mobility of Au atoms. Thus, these Au atoms distributed in slag phase may be readily transferred into iron phase to form Fe-rich ( $\gamma$ -Fe) phase due to high mobility. Therefore, with the increase of reduction temperature, more gold in cyanide tailings could be allocated into iron phase rather than in slag phase.

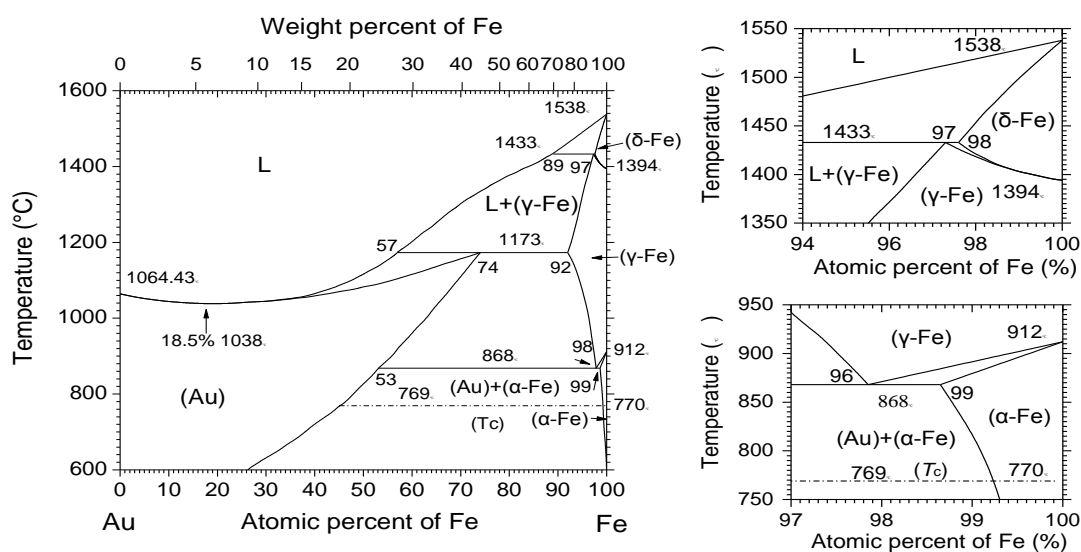


Figure 6. Phase diagram of Au-Fe binary system.

Figure 7 showed XRD patterns of roasted products obtained from 1050 to 1250 °C. Metallic iron was generated even at 1050 °C. The intensity of diffraction peaks assigned to metallic iron became strong, revealing higher amount and larger crystal size of metallic iron at elevated temperature. As shown in Figure 8, the grain size of metallic iron (grayish white) at 1050 °C was just about 20  $\mu\text{m}$ , and most of these grains were separated. Nevertheless, some grain size of metallic iron at 1200 °C was increased up to about 100  $\mu\text{m}$  and dispersed metallic iron particles had been aggregated into larger grains. Herein, it should point out that metallic iron grains containing gold is recovered by the grinding and magnetic separation process. The larger grain size means easy separation of iron grains from the slags by the physical separation method such as magnetic separation. Therefore, as shown in Figure 3, the higher Au and Fe recovery of iron powders was observed.

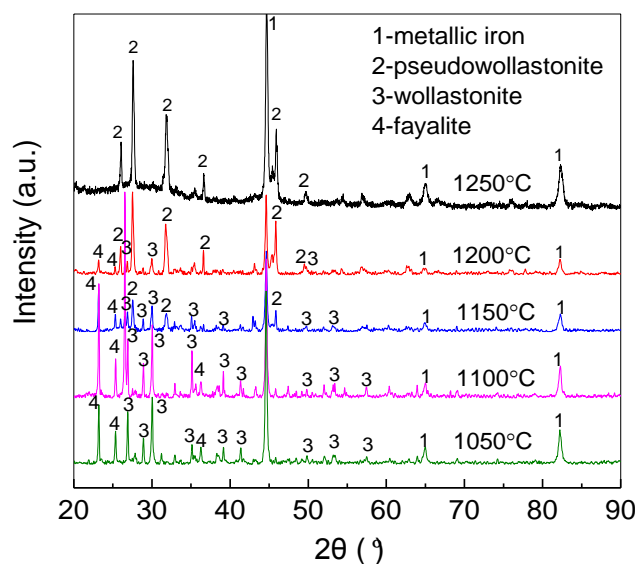
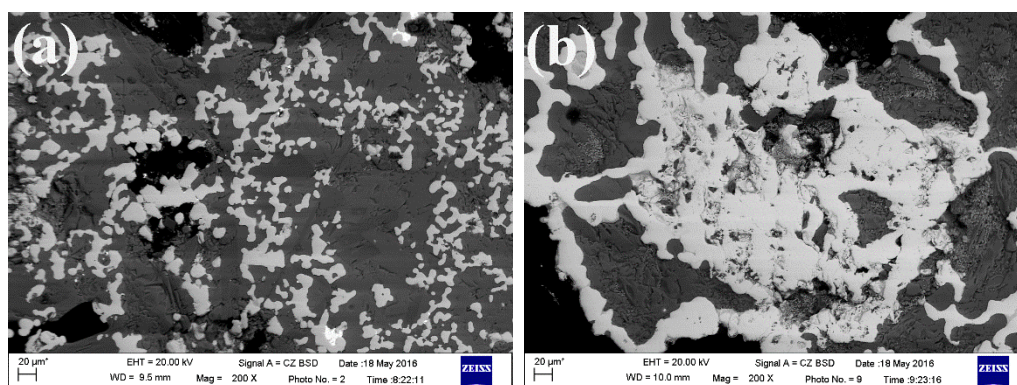


Figure 7. XRD patterns of roasted products obtained at different roasting temperatures.



**Figure 8.** SEM images of roasted products obtained at 1050°C (a) and 1200°C (b) with same magnification of 200.

As shown in Figure 7, as the roasting temperature was increased, the fayalite, a low melting point material, had lower fraction in slag phase and disappeared at 1250 °C. At the same time, more wollastonite ( $\alpha$ -CaSiO<sub>3</sub>) in slag phase was transformed to pseudowollastonite ( $\beta$ -CaSiO<sub>3</sub>) at temperature higher than 1150 °C since the transformation temperature of  $\alpha$ -CaSiO<sub>3</sub> to  $\beta$ -CaSiO<sub>3</sub> was 1126 °C. Compared to fayalite (melting point of 1205 °C), (pseudo)wollastonite had the higher melting point of 1540 °C [35]. Thus, the amount of liquidus in reduction system would remarkable decrease as more pseudowollastonite was generated at higher reduction temperature, preventing the mechanical mixing of molten gold in slag phase. Thus, more gold can be allocated into iron phase to form Au-Fe alloy. It was well in agreement with higher Au recovery at elevated temperature (Figure 3) and with increased CaO dosage (Figure 5).

### 3.3. Sulfuric Acid Leaching of Gold Containing Iron Powders

Sulfuric acid leaching was used to separate gold and iron in iron powders. The effect of leaching temperature on iron dissolution was shown in Figure 9. As the temperature was raised from 30 to 50 °C, the weight loss ratio and iron leaching rate were increased from 71.41% to 96.20% and from 82.97% to 98.82%, respectively. While the temperature was further raised to 90 °C, the iron leaching rate became almost constant. At acid-leaching temperature of 50 °C, the yield of acid-leaching residue to cyanide tailings was reduced to 1.72%, and the gold grade reached as high as 216.58 g/t (Figure 1), revealing remarkable gold enrichment and significant weight decrease of acid-leaching residue.

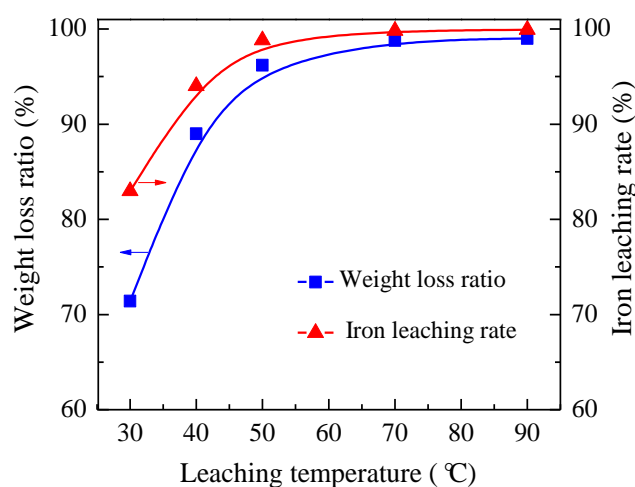


**Figure 9.** Effect of acid-leaching temperature on iron dissolution of reduced iron powders.

Figure 10 showed XRD pattern of acid-leaching residue. The diffraction peaks could be assigned to cohenite ( $\text{Fe}_3\text{C}$ ) and bustamite ( $\text{CaMn}(\text{SiO}_3)_2$ ), generated in the direct reduction roasting. A broad peak with a  $2\theta$  degree of  $10\text{--}40^\circ\text{C}$  was observed, indicating the appearance of amorphous materials. However, no diffraction peak of metallic iron was observed, revealing nearly complete dissolution of metallic iron in dilute  $\text{H}_2\text{SO}_4$  solution at  $50^\circ\text{C}$ . Therefore, it can reasonably infer that the Au-Fe alloy structure in iron powders must be completely broken, and gold should be fully exposed in acid-leaching residue. In this work, metallic iron in iron powders was found to readily react with dilute  $\text{H}_2\text{SO}_4$  to produce  $\text{FeSO}_4$  at  $50^\circ\text{C}$  according to Equations (9–11). However, sulfuric acid leaching of iron oxides (e.g., hematite) should be conducted at much higher temperature ( $90\text{--}110^\circ\text{C}$ ) and with longer time (2–4 h) [44,45].

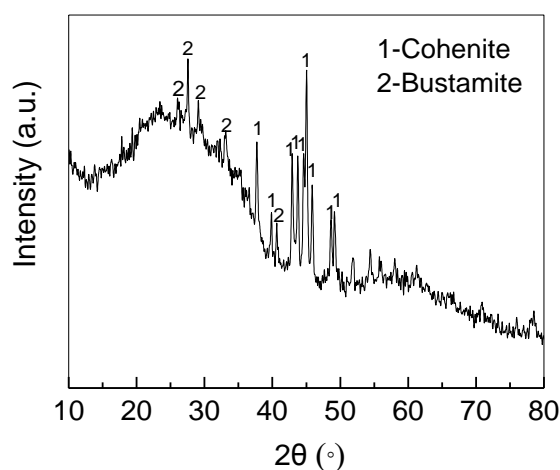
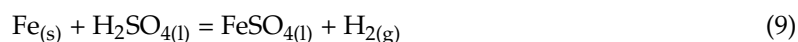


Figure 10. XRD pattern of acid-leaching residue.

The ferrous sulfate in leachate was recovered to produce  $\text{FeSO}_4 \cdot 7\text{H}_2\text{O}$  crystals with a low temperature crystallization process. The yield of  $\text{FeSO}_4 \cdot 7\text{H}_2\text{O}$  to cyanide tailings was as high as 222.42% as shown in Figure 1. The chemical composition in Table 2 showed that the content of  $\text{FeSO}_4 \cdot 7\text{H}_2\text{O}$  reached 96.73% with low content of harmful elements such as Pb and As. The obtained  $\text{FeSO}_4 \cdot 7\text{H}_2\text{O}$  crystals can be used as raw materials in the production of pigment, water treatment chemicals and feed for animals, etc.

Table 2. Chemical composition of prepared  $\text{FeSO}_4 \cdot 7\text{H}_2\text{O}$  crystals.

Components	$\text{FeSO}_4 \cdot 7\text{H}_2\text{O}$	Mn	Pb	As	Si	Al	Cu
Content (%)	96.73	0.011	0.002	0.0001	0.03	0.01	0.003

### 3.4. Recovery of Gold from Acid-Leaching Residue

The enriched gold in acid-leaching residue was finally extracted by the cyanidation extraction. As given in Table 3, the gold extraction rate was increased at higher cyanide dosage. At the cyanide dosage of 40 kg/t, the extraction rate was increased up to 96.72%, which revealed nearly complete exposure of gold in acid-leaching residue. The gold in pregnant solution was not further recovered at the current stage, and further studies such as adsorption by activated carbon or ion exchange of gold would be taken. As shown in Figure 1, the gold grade of produced cyanide residue reached 7.10 g/t,

which could be recycled into the direct reduction roasting as raw materials. Therefore, there was no toxic secondary cyanide residue produced in this process.

**Table 3.** The gold extraction rate of acid-leaching residue.

Cyanide Dosage (kg/t)	5	10	20	40	80
Gold extraction rate (%)	56.78	87.46	94.48	96.72	96.93

In this work, the total gold recovery of whole process, i.e., gold recovery in direct reduction roasting (97.46%)  $\times$  gold extraction rate (96.72%), was as high as 94.23%, showing high gold recovery of this combined process in treating cyanide tailings. As the gold in acid-leaching residue was fully exposed and had high grade of 216.58 g/t, the cyanide consumption per unit weight of gold was as low as 0.185 kg (NaCN)/g(gold). However, for gold ores (e.g., gold grade of 2 g/t), the cyanide consumption usually reaches 0.5–1 kg (NaCN)/g (gold) for the huge amount of ores although the cyanide dosage (1–2 kg/t) is much lower than that in this work (Table 3) [46]. Thus, it was worthwhile noting that the cyanide consumption in this process was much lower than that in gold extraction industries.

#### 4. Conclusions

In this work, the combined direct reduction roasting and leaching process could effectively recover gold and iron from cyanide tailings discharged after the roasting-cyanidation leaching. The effects of direct reduction parameters on the gold enrichment were studied. Gold containing iron powders, i.e., Fe-rich Au-Fe alloy, were produced by the direct reduction roasting-magnetic separation. Under the optimum conditions—reduction temperature of 1200 °C, reduction time of 90 min, coal dosage of 20 wt.% and CaO dosage of 20 wt.%—the TFe content and recovery of iron powders reached 92.43% and 93.21%, respectively, and the gold grade and recovery reached 8.23 g/t and 97.46%, respectively. The magnetic separation tailings, with a yield of 51.33% to cyanide tailings, had no toxic cyanides any more. The gold and iron in iron powders were further separated by sulfuric acid leaching. The leachate was used to prepared FeSO<sub>4</sub>·7H<sub>2</sub>O crystals with a yield of 222.42% to cyanide tailings. The acid-leaching residue with the gold grade of 216.58 g/t was subjected to the cyanidation extraction with gold extraction rate of 96.72%. The total gold recovery of whole process was as high as 94.23%. The cyanide residue generated could be recycled into direct reduction roasting as gold containing raw materials.

The increase of reduction temperature, coal dosage and CaO dosage resulted in higher Au recovery in iron powders. The higher dosage of coal and CaO promoted the reduction of fayalite to metallic iron and increased the melting temperature of slag phase, which enhanced more gold allocated in iron phase rather than in slag phase.

As the mineralogical properties of cyanide tailings after the roasting-cyanidation leaching were close to that of pyrite cinders and gold containing iron ores, the novel process investigated could be applied in valuable metal recovery from these tailings and natural ores. However, in this work, the enrichment of silver in cyanide tailings into iron powders had not been studied. In the future work, the enrichment behaviors of silver in the direct reduction should be fully investigated.

**Author Contributions:** P.F. designed the experiments and prepared the manuscript. Z.L. conducted the XRD and SEM tests. F.J. performed the experiments of direct reduction roasting, magnetic separation and acid leaching. Z.B. conducted the cyanidation extraction and analyzed the element contents of samples.

**Funding:** This research was funded by the National Natural Science Foundation of China, grant number 51674017.

**Acknowledgments:** The authors would like to appreciate the China Scholarship Council for funding the State Scholarship, grant number 201706465070, and thank to Experiment Center in School of Metallurgical and Ecological Engineering, University of Science and Technology Beijing for providing access to analytical facilities.

**Conflicts of Interest:** The authors declare no conflict of interest.

## References

1. Sayiner, B. Influence of lead nitrate on cyanide leaching of gold and silver from Turkish gold ores. *Physicochem. Probl. Miner. Process.* **2014**, *50*, 507–513. [[CrossRef](#)]
2. Yazici, E.Y.; Ahlatci, F.; Koc, E.; Celep, O.; Devenci, H. Pre-treatment of a copper-rich gold ore for elimination of copper interference. In Proceedings of the European Metallurgical Conference, Weimar, Germany, 23–26 June 2016.
3. Donato, D.B.; Nichols, O.; Possingham, H.; Moore, M.; Ricci, P.F.; Noller, B.N. A critical review of the effects of gold cyanide-bearing tailings solutions on wildlife. *Environ. Int.* **2007**, *33*, 974–984. [[CrossRef](#)] [[PubMed](#)]
4. Zhong, Q.; Yang, Y.B.; Chen, L.J.; Li, Q.; Xu, B.; Jiang, T. Intensification behavior of mercury ions gold cyanide leaching. *Metals* **2018**, *8*, 80. [[CrossRef](#)]
5. Clement, A.J.H.; Novakova, T.; Hudson-Edwards, K.A.; Fuller, I.C.; Macklin, M.G.; Fox, E.G.; Zapico, I. The environmental and geomorphological impacts of historical gold mining in the Ohinemuri and Waihou river catchments, Coromandel, New Zealand. *Geomorphology* **2017**, *295*, 159–175. [[CrossRef](#)]
6. Koohestani, B.; Darban, A.K.; Darezereshki, E.; Mokhtari, P.; Yilmaz, E.; Yilmaz, E. The influence of sodium and sulfate ions on total solidification and encapsulation potential of iron-rich acid mine drainage in silica gel. *J. Environ. Chem. Eng.* **2018**, *6*, 3520–3527. [[CrossRef](#)]
7. Yilmaz, E.; Ahlatci, F.; Yazici, E.Y.; Celep, O.; Devenci, H. Passivation of pyritic tailings and mitigation of its acid mine drainage (AMD) potential. In Proceedings of the International Symposium on Mining and Environment, Mugla, Turkey, 27–29 September 2017.
8. Zhang, Y.L.; Li, H.M.; Yu, X.J. Recovery of iron from cyanide tailings with reduction roasting-water leaching followed by magnetic separation. *J. Hazard. Mater.* **2012**, *213–214*, 167–174. [[CrossRef](#)] [[PubMed](#)]
9. Liu, B.L.; Zhang, Z.H.; Li, L.B.; Wang, Y.J. Recovery of gold and iron from the cyanide tailings by magnetic roasting. *Rare Metal. Mater. Eng.* **2013**, *42*, 1805–1809.
10. Piłśniak-Rabiega, M.; Trochimczuk, A.W. Selective recovery of gold on functionalized resins. *Hydrometallurgy* **2014**, *146*, 111–118. [[CrossRef](#)]
11. De Andrade Lima, L.R.P.; Bernardes, L.A.; Barbosa, L.A.D. Characterization and treatment of artisanal gold mine tailings. *J. Hazard. Mater.* **2008**, *150*, 747–753. [[CrossRef](#)] [[PubMed](#)]
12. Syed, S. Recovery of gold from secondary sources—A review. *Hydrometallurgy* **2012**, *115–116*, 30–51. [[CrossRef](#)]
13. Koc, E.; Ahlatci, F.; Kuzu, M.; Yazici, E.Y.; Celep, O.; Devenci, H. Recovery of silver from cyanide leach solutions of a pyritic gold concentrate by sodium sulphide precipitation. In Proceedings of the 15th International Mineral Processing Symposium and Exhibition, Istanbul, Turkey, 11–13 June 2016.
14. Yazici, E.Y.; Yilmaz, E.; Ahlatci, F.; Celep, O.; Devenci, H. Recovery of silver from cyanide leach solutions by precipitation using Trimercapto-s-triazine (TMT). *Hydrometallurgy* **2016**, *174*, 175–183. [[CrossRef](#)]
15. Ilankoon, I.M.S.K.; Tang, Y.; Ghorbani, Y.; Northey, S.; Yellishetty, M.; Deng, X.Y.; McBride, D. The current state and future directions of percolation leaching in the Chinese mining industry: Challenges and opportunities. *Miner. Eng.* **2018**, *125*, 206–222. [[CrossRef](#)]
16. Dehghani, A.; Ostad-rahimi, M.; Mojtahedzadeh, S.H.; Gharibi, K.K. Recovery of gold from the mouteh gold mine tailings dam. *J. South African Inst. Min. Metall.* **2009**, *109*, 417–421.
17. Lv, C.C.; Ding, J.; Qian, P.; Li, Q.C.; Ye, S.F.; Chen, Y.F. Comprehensive recovery of metals from cyanidation tailing. *Miner. Eng.* **2015**, *70*, 141–147. [[CrossRef](#)]
18. Yang, X.L.; Huang, X.; Qiu, T.S. Recovery of zinc from cyanide tailings by flotation. *Miner. Eng.* **2015**, *84*, 100–105. [[CrossRef](#)]
19. Li, D.X.; Gao, G.L.; Meng, F.L.; Ji, C. Preparation of nano-iron oxide red pigment powders by use of cyanided tailings. *J. Hazard. Mater.* **2008**, *155*, 369–377. [[CrossRef](#)]
20. Bas, A.D.; Safizadeh, F.; Ghali, E.; Choi, Y. Leaching and electrochemical dissolution of gold in the presence of iron oxide minerals associated with roasted gold ore. *Hydrometallurgy* **2016**, *166*, 143–153. [[CrossRef](#)]
21. Li, Z.Y.; Wang, W.W.; Yue, K.; Chen, M.X. High-temperature chlorination of gold with transformation of iron phase. *Rare Met.* **2016**, *35*, 881–886. [[CrossRef](#)]
22. Li, H.Y.; Zhang, L.B.; Koppala, S.; Ma, A.Y.; Peng, J.H.; Li, S.W.; Yin, S.H. Extraction of gold and silver in the selective chlorination roasting process of cyanidation tailing. *Sep. Sci. Technol.* **2018**, *53*, 458–466. [[CrossRef](#)]
23. Okamoto, H.; Massalski, T.B.; Swartzendruber, L.J.; Beck, P.A. The Au-Fe (gold-iron) system. *Bull. Alloy Phase Diagrams* **1984**, *5*, 592–601. [[CrossRef](#)]

24. Bansal, C.; Sarkar, S.; Mishra, A.K.; Abraham, T.; Lemier, C.; Hahn, H. Electronically tunable conductivity of a nanoporous Au–Fe alloy. *Scr. Mater.* **2007**, *56*, 705–708. [[CrossRef](#)]
25. Lee, Y.P.; Kudryavtsev, Y.V.; Nemoshkalenko, V.V.; Gontarz, R.; Rhee, J.Y. Magneto-optical and optical properties of Fe-rich Au-Fe alloy films near the fcc-bcc structural transformation region. *Phys. Rev. B* **2003**, *67*, 104424. [[CrossRef](#)]
26. Konieczny, R.; Idczak, R.; Chojcan, J. A study of thermodynamic properties of dilute Fe-Au alloys by the <sup>57</sup>Fe Mössbauer Spectroscopy. *Acta Phys. Pol. A* **2017**, *131*, 255–258. [[CrossRef](#)]
27. Kumar, P.S.M.; Sivakumar, T.; Fujita, T.; Jayavel, R.; Abe, H. Synthesis of metastable Au-Fe alloy using ordered nanoporous silica as a hard template. *Metals* **2018**, *8*, 17. [[CrossRef](#)]
28. Xiang, J.Y.; Huang, Q.Y.; Lv, X.W.; Bai, C.G. Multistage utilization process for the gradient-recovery of V, Fe, and Ti from vanadium-bearing converter slag. *J. Hazard. Mater.* **2017**, *336*, 1–7. [[CrossRef](#)] [[PubMed](#)]
29. Yang, H.F.; Jing, L.L.; Zhang, B.G. Recovery of iron from vanadium tailings with coal-based direct reduction followed by magnetic separation. *J. Hazard. Mater.* **2011**, *185*, 1405–1411. [[CrossRef](#)] [[PubMed](#)]
30. Cao, Z.C.; Sun, T.C.; Xue, X.; Liu, Z.H. Iron recovery from discarded copper slag in a RHF direct reduction and subsequent grinding/magnetic separation process. *Minerals* **2016**, *6*, 119. [[CrossRef](#)]
31. Zhang, B.J.; Niu, L.P.; Zhang, T.G.; Li, Z.Q.; Zhang, D.L.; Zheng, C. Alternative reduction of copper matte in reduction process of copper slag. *ISIJ Int.* **2017**, *57*, 775–781. [[CrossRef](#)]
32. Li, W.F.; Zhan, J.; Fan, Y.Q.; Wei, C.; Zhang, C.F.; Hwang, J.Y. Research and industrial application of a process for direct reduction of molten high-lead smelting slag. *JOM* **2017**, *69*, 784–789. [[CrossRef](#)]
33. Xu, B.; Kong, W.H.; Li, Q.; Yang, Y.B.; Jiang, T.; Liu, X.L. A review of thiosulfate leaching of gold: Focus on thiosulfate consumption and gold recovery from pregnant solution. *Metals* **2017**, *7*, 222. [[CrossRef](#)]
34. Ahtiainen, R.; Lundstrom, M. Preg-robbing of gold in chloride-bromide solution. *Physicochem. Probl. Miner. Process.* **2016**, *52*, 244–251. [[CrossRef](#)]
35. Liu, G.S.; Strezov, V.; Lucas, J.A.; Wibberley, L.J. Thermal investigations of direct iron ore reduction with coal. *Thermochim. Acta* **2004**, *410*, 133–140. [[CrossRef](#)]
36. Li, Y.L.; Sun, T.C.; Kou, J.; Guo, Q.; Xu, C.Y. Study on phosphorus removal of high-phosphorus oolitic hematite by coal-based direct reduction and magnetic separation. *Min. Proc. Ext. Met. Rev.* **2014**, *35*, 66–73. [[CrossRef](#)]
37. Han, H.; Duan, D.; Yuan, P.; Chen, S. Recovery of metallic iron from high phosphorous oolitic hematite by carbothermic reduction and magnetic separation. *Ironmak. Steelmak.* **2015**, *42*, 542–547. [[CrossRef](#)]
38. Yu, W.; Tang, Q.Y.; Chen, J.A.; Sun, T.C. Thermodynamic analysis of the carbothermic reduction of a high-phosphorus oolitic iron ore by FactSage. *Int. J. Min., Met. Mater.* **2016**, *23*, 1126–1132. [[CrossRef](#)]
39. Yu, W.; Sun, T.C.; Cui, Q.; Xu, C.Y.; Kou, J. Effect of coal type on the reduction and magnetic separation of a high-phosphorus oolitic hematite ore. *ISIJ Int.* **2015**, *55*, 536–543. [[CrossRef](#)]
40. Zhou, X.L.; Zhu, D.Q.; Pan, J.; Wu, T.J. Utilization of waste copper slag to produce directly reduced iron for weathering resistant steel. *ISIJ Int.* **2015**, *55*, 1347–1352. [[CrossRef](#)]
41. Cheng, X.L.; Zhao, K.; Qi, Y.H.; Shi, X.F.; Zheng, C.L. Direct reduction experiment on iron-bearing waste slag. *J. Iron Steel Res. Int.* **2013**, *20*, 24–29. [[CrossRef](#)]
42. Mousa, E.A. Effect of basicity on wustite sinter reducibility under simulated blast furnace conditions. *Ironmak. Steelmak.* **2014**, *41*, 418–429. [[CrossRef](#)]
43. Favez, D.; Wagnière, J.D.; Rappaz, M. Au-Fe alloy solidification and solid-state transformations. *Acta Mater.* **2010**, *58*, 1016–1025. [[CrossRef](#)]
44. Liu, Z.R.; Zeng, K.; Zhao, W.; Li, Y. Effect of temperature on iron leaching from bauxite residue by sulfuric acid. *Bull. Environ. Contam. Toxicol.* **2009**, *82*, 55–58. [[CrossRef](#)] [[PubMed](#)]
45. Zheng, Y.J.; Liu, Z.C. Preparation of monodispersed micaceous iron oxide pigment from pyrite cinders. *Powder Technol.* **2011**, *207*, 335–342. [[CrossRef](#)]
46. Bas, A.D.; Koc, E.; Yazici, E.Y.; Deveci, H. Treatment of copper-rich gold ore by cyanide leaching, ammonia pretreatment and ammoniacal cyanide leaching. *Trans. Nonferrous Met. Soc. China* **2015**, *25*, 597–607. [[CrossRef](#)]

